Optimization preparation of activated carbon from *Enteromorpha prolifra* using response surface methodology and its adsorption studies of fluoroquinolone antibiotics

Yuan Gao, Qinyan Yue*, Baoyu Gao, Yuanyuan Sun

Shandong Provincial Key Laboratory of Water Pollution Control and Resource Reuse, School of Environmental Science and Engineering, Shandong University, Jinan 250100, China, Tel. +86 15169056115; email: gy_1988@aliyun.com (Y. Gao), Tel. +86 531 88365258; Fax: +86 531 88364513; email: qyyue58@aliyun.com (Q. Yue), Tel. +86 531 88366771; email: baoyugao_sdu@aliyun.com (B. Gao), Tel. +86 15866634850; email: sunyuan870102@163.com (Y. Sun)

ABSTRACT

Enteromorpha prolifera, a marine solid waste abundantly available in Asia, was used as a low-cost precursor to prepare activated carbon (EPAC) using pyrophosphoric acid, $H_4P_2O_7$, as a chemical activating agent. The effects of impregnation ratio, activation temperature and activation time on the specific surface area of the activated carbon were investigated through response surface methodology. The optimum preparation conditions were described as follows: impregnation ratio, 1.26; activation temperature, 455°C; activation time, 48 min. The characteristics of EPAC were examined by nitrogen adsorption–desorption isotherms, Fourier transformed infrared spectroscopy and scanning electron microscopy. The total pore volume and specific surface area of EPAC under optimum conditions were identified as 1.365 cm^3/g and 1124.1 m^2/g. The EPAC possessed high BJH pore volume, 1.276 cm^3/g and methylene blue value, 330 mg/g, indicating the existence of abundant mesopores. The adsorption kinetic data of ciprofloxacin were well fitted to pseudo-second-order model, displaying a monolayer adsorption capacity for CIP of 216.55 mg/g. The equilibrium data can be well described by Langmuir model. The dominant sorption mechanism is electrostatic attraction.

Keywords: Enteromorpha prolifera; Response surface methodology; Fluoroquinolone antibiotics; Adsorption mechanism

1. Introduction

In recent years, large-scale break-out of algae has led to ecological impacts including destruction of coastal marine habitats, reduction of biodiversity, economic losses in marine industries and uncoupled biogeochemical cycles [1]. *Enteromorpha prolifra (E. prolifra),* a green algae, appeared in an unprece-dented scale near the shore of Asia-Pacific region [2]. In summer 2008, 100 million metric tons of *E. prolifra* bloomed along the shore of Qingdao (China) and it is estimated that 1,000 million metric tons of *E. prolifra* blooms occurred in Yellow sea, which has a serious impact on local ocean transportation, water quality and tourism, especially on the forthcoming Olympic sailing competition in Qingdao at that time [1,3,4]. The same blooms appeared again in 2009, 2011, 2012 and 2013 (Xinhua News), indicating the *E. prolifra* tides have

*Corresponding author.

turned into a recurrent phenomenon in that region. Generally, most of *E. prolifra* are abandoned and only partial *E. prolifra* is used as pharmaceutical product, livestock feed and fertilizer. Therefore, it is urgent to find a feasible technology to utilize this waste effectively. The main ingredient of *E. prolifra* is hemicellulose [2], which gives *E. prolifra* a huge potential to be a low-cost activated carbon precursor. In addition, *E. prolifra* contains abundant sulphate, hydroxyl, carboxyl and amino functional groups and these unique physico-chemical properties make it an ideal alternative as binding sites for contaminants [5,6].

Generally, two different methods are used for the preparation of activated carbon, namely physical and chemical activation [5,7]. Compared to physical activation, chemical activation can be controlled easily, operated at relatively low reaction temperature and shorter reaction time [5]. The common dehydrating activating agents are considered to be $ZnCl_2$ [5,8,9], H_3PO_4 [10,11], NaOH [12,13] and KOH [14–16]. As an unconventional activating agent, pyrophosphoric acid ($H_4P_2O_7$) has received some attention mainly due to its role in considerably increasing mesopore ratio of the resultant carbons. Liu et al. discussed the influences of $H_xP_yO_z$ species transformed by H_3PO_4 on the carbons [17]. Sun et al. reported the comparison of *arundo donax Linn* derived carbons with $H_4P_2O_7$ activation via conventional and microwave heating methods [18]. However, there are no reports on the optimal preparation of *E. prolifra*-based carbons by $H_4P_2O_7$ activation. Therefore, it is necessary to investigate the effects of activation conditions on the *E. prolifra*-derived carbons. Furthermore, the preparation of *E. prolifra*-derived carbons not only introduces a novel treatment method for this waste material, but also provides a renewable and cheaper raw precursor for the preparation of carbons. Ciprofloxacin, as one of the most common fluoroquinolone antimicrobials in water, can lead to the spread of antibiotic-resistant bacteria, disrupting of hormone features and ecosystem function. Therefore, ciprofloxacin (CIP) was chosen to be a targeted pollutant in this study.

The aim of this work was to systematically investigate the effects of each condition and the interactions of the conditions on specific surface area of the prepared carbon via response surface methodology. Moreover, the adsorption properties and mechanism of the carbons toward ciprofloxacin was evaluated.

2. Materials and methods

2.1. Raw material

E. prolifra, obtained from Qingdao, Shandong, China, was washed with deionized water to remove dust and impurities, and then dried at 70°C for 12 h to remove surface water. Finally, the cleaned *E. prolifra* was crushed using a grinder crusher and sieved to desired size (75–2000 μm). CIP (supplied by Sangon Biotech, Shanghai, China) of purity 99.6% was used as an adsorbate. The other reagents were all of analytical grade.

2.2. Preparation of activated carbon

E. prolifra was firstly mixed with pyrophosphoric acid at different mass ratio and soaked for 12 h. Subsequently, the mixture was placed in a chamber electric furnace (KSY-4D-16), heated to desired temperature at a heat rate of 10°C/min and maintained for different activation time. After cooling to the room temperature, the samples were washed with deionized water until the pH of the supernatant became stable (7.0 ± 0.5). Afterwards, the activated products were dried, crushed and sifted to obtain desired powder with a particle size of 75–150 μm for the following experiments.

2.3. Experimental design and statistical analysis

In this study, a classical RSM design, known as Box and Behnken design (BBD) was applied to investigate the interactions of each variable in order to find the optimum conditions for the preparation of *E. prolifra* based activated carbon. RSM, a useful mathematical and statistical technique, has been applied widely for the optimization of experimental conditions [19,20]. The total number of experiments T_n is calculated according to the following equation:

$$T_n = 2^n + 2n + 1 \tag{1}$$

Therefore, a total of 17 experiments were contained in this design, including five repeated experiments observations at the central point, to evaluate the experimental error. The quadratic equation model was applied to predicate the experimental observations. The model was expressed as follows:

$$y = a_0 + \sum a_i x_i + \sum a_{ii} x_{ii}^2 + \sum a_{ij} x_i x_j \tag{2}$$

where y is the predicted response, a_0 is the constant coefficient, a_i is the linear coefficient, a_{ii} is the quadratic coefficient, a_{ij} is the different interaction coefficient and x_i and x_j are the coded independent variables. The statistical significance, regression analysis and response surfaces were obtained to

predict the optimum preparation conditions resulting in maximum specific surface area of activated carbon. The analysis of variance (ANOVA) was conducted to evaluate the statistical significance of variables. F-test, correlation coefficient (R^2) and amendatory correlation coefficient (R_{adj}^2) were used to express the quality of fit of the model.

2.4. Characterization of activated carbon

The prepared carbons under optimum conditions were characterized to identify its texture properties and chemical characters. The textural characterization of EPAC was carried out using N_2 adsorption–desorption isotherms at 77 K by an automated pore size and surface area analyser (JW-BK122 W). The samples were pretreated by heating at 200°C under vacuum condition for 120 min to remove surface water and other impurity gases. For the measurement data, the specific surface area (S_{BET}) was obtained by Brunauer–Emmett–Teller equation. The micropore surface area (S_{mic}) and micropore volume (V_{mic}) were analysed by t-plot method. The total pore volume was obtained according to the amount of nitrogen adsorbed at the relative pressure $P/P_0 = 0.99$. The average pore size was calculated based on the equation $D_{AC} = 4 V/S_{BET}$. The external volume (V_{ext}) was calculated by deducting V_{mic} from V_{tot} and the external area (S_{ext}) was calculated by deducting S_{mic} from S_{tot}.

The morphological features of EPAC were observed by scanning electron microscope (SEM Hitachi S-520, Japan). The surface functional groups of activated carbon were recorded by Fourier transformed infrared spectroscopy (Avatar 370) and the spectra were varied from 400 to 4,000 cm^{-1}. The zeta potentials of the samples were determined using Zetaplus Particle apparatus (JS94H, China). Adsorption experiment was performed by agitating 0.1 g of adsorbent with certain amount of methylene blue solution in 100 mL Erlenmeyer flasks at 20 ± 5°C for 25 min. Then, the supernatant solution was filtered using filter paper to determine the residual dye concentration by spectrophotometric method at $\lambda_{max} = 665$ nm. The absorbance value was compared with that of 0.4% copper sulfate solution. The dosage of methylene blue was changed until the deviation between those two values was less than 0.02. The consumed amount of methylene blue was considered to be the so-called methylene blue value.

2.5. Ciprofloxacin adsorption

The adsorption experiments of CIP were performed in order to evaluate the adsorptive capacity of the prepared activated carbon. The adsorption kinetic experiments were performed at room temperature with different initial CIP concentration of 101, 199 and 289 mg/L, respectively. The 250 mL Erlenmeyer flasks containing 0.05 g activated carbon and 50 mL various initial concentrations of CIP solution were used to carry out the kinetic experiment. The flasks were placed on a constant temperature bath oscillator with a speed of 150 rpm. Small volumes of samples were periodically withdrawn and filtered with a 0.45 μm micro-pore membrane. The concentrations were measured by UV-visible spectrophotometer (TU-1810, Beijing) at maximum absorbance wavelength, ($\lambda_{max} = 270$ nm) according to the previous research [21]. The final sample was maintained for enough time to ensure adsorption equilibrium and the adsorption experiments were performed in triplicate so as to reduce errors. Adsorption isotherms experiments were conducted with CIP concentration ranging from 50 to 500 mg/L. The initial pH values of CIP solution were adjusted with sodium hydroxide or hydrochloric acid solution. The amount of CIP absorbed per unit mass of the sorbents, q_e was calculated by:

$$q_e = \frac{(C_0 - C_e)}{M} \cdot V \qquad (3)$$

where M (g) was the mass of adsorbents and V (L) was the volume of CIP solution. C_e (mg/L) and C_0 (mg/L) were the equilibrium and initial concentrations of CIP, respectively.

3. Results and discussion

3.1. Preparation of activated carbon using BBD model

3.1.1. Development of regression model equation

BBD was used to develop the correlations between the preparation variables (including impregnation ratio, activation temperature and activation time) and the specific surface area. Table 1 shows the design matrices together with the response values obtained through the practical experiments. The specific surface area was found to vary from 620 to 1,110 m^2/g. The quadratic models were selected to fit the response function, as suggested by the Design Expert 7.0 software. The final models in terms of coded and actual factors were shown as follows:

$$\begin{aligned} y_2(\text{coded}) = {} & 1,095 + 136.5x_1 - 13.12x_2 - 70.13x_3 \\ & - 2x_1x_2 + 75x_1x_3 - 45.75x_2x_3 - 69.63x_1^2 \\ & - 128.88x_2^2 - 90.87x_3^2 \end{aligned}$$

$$\qquad (4)$$

Table 1
Experimental design matrix of Box-Behnken design.

Runs	Levels			Activated carbon preparation variables			Response (BET specific surface area (m^2/g))
				Ratio	Activation temperature (°C)	Activation time (min)	
1	−1	0	−1	0.45	450	30	984
2	0	0	0	0.90	450	60	1,106
3	0	+1	−1	0.90	500	30	957
4	−1	−1	0	0.45	400	60	783
5	+1	0	−1	1.35	450	30	1,099
6	0	0	0	0.90	450	60	1,085
7	0	+1	1	0.90	500	90	799
8	0	−1	−1	0.90	400	30	860
9	0	0	0	0.90	450	60	1,094
10	0	−1	+1	0.90	400	90	885
11	−1	0	+1	0.45	450	90	620
12	−1	+1	0	0.45	500	60	729
13	0	0	0	0.90	450	60	1,110
14	0	0	0	0.90	450	60	1,080
15	+1	0	+1	1.35	450	90	1,035
16	+1	−1	0	1.35	400	60	1,068
17	+1	+1	0	1.35	500	60	1,006

$$y_2(\text{actual}) = -10,560 + 628.89x_1 + 48.04x_2 + 18.50x_3$$
$$- 0.089x_1x_2 + 5.56x_1x_3 - 0.031x_2x_3$$
$$- 343.83x_1^2 - 0.052x_2^2 - 0.10x_3^2$$

$$(5)$$

Positive and negative signs prefixing the terms indicated the synergistic and antagonistic effect, respectively. The correlation coefficient (R^2) and amendatory correlation coefficient (R_{adj}^2) were introduced to evaluate the quality of the model, which were 0.9633 and 0.9161. The R^2 and R_{adj}^2 were relatively high, indicating an excellent agreement between the model prediction and the experimental data. Fig. 1 shows the experimental values were close to the predicted values, implying the developed model was good at capturing the correlation between the preparation variables and specific surface area.

The ANOVA for the quadratic model is listed in Table 2. The model F-value of 20.4 implied the model was significant. In this study, the values of Prob. > F less than 0.05 illustrated the model terms were significant. It was found that all three variables were indirectly and directly involved in enriching the specific surface area. Among all the variables, impregnation ratio was found to have the largest influence (thanks to the highest value of F), and the interaction between the impregnation ratio and activation time had considerable influence on the production of EPAC with higher specific surface area compared to other interactions. The activation time has considerable
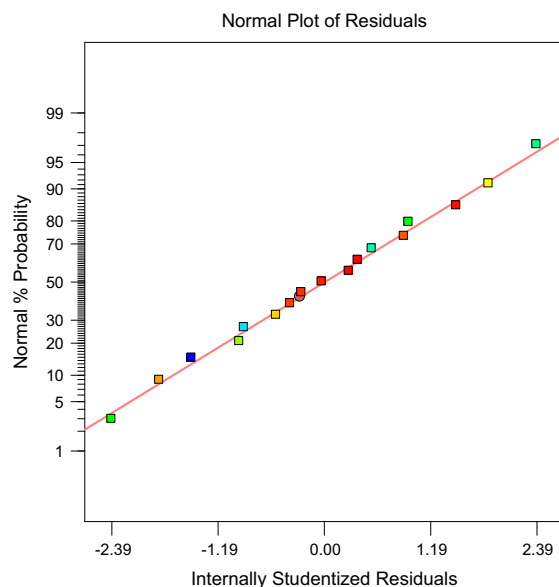
Fig. 1. Predicted versus experimental specific surface area of EPAC.

influence on the specific surface area too, second in importance. Otherwise, the activation temperature and interaction between impregnation ratio and activation temperature have least significant influence on the specific surface area. Hence, the influence of variables on the specific surface area was in the order: impregnation ratio > activation time > the interaction between

Table 2
Variance analysis of response surface quadratic model for BET specific surface area

Source	Sum of squares	Degree of freedom	Mean square	F value	Prob. $>F$
Model	359,200	9	39,914.02	20.40	0.0003
x_1	149,100	1	149,100	76.19	<0.0001
x_2	1,378.13	1	1,378.13	0.7	0.4290
x_3	39,340.13	1	39,340.13	20.11	0.0029
$x_1 x_2$	16.00	1	16.00	0.0082	0.9305
$x_1 x_3$	22,500	1	22,500	11.50	0.0116
$x_2 x_3$	8,372.25	1	8,372.25	4.28	0.0774
x_1^2	20,411.12	1	20,411.12	10.43	0.0145
x_2^2	69,931.64	1	69,931.64	35.75	0.0006
x_3^2	34,771.64	1	34,771.64	17.77	0.0040
Residual	13,694.25	7	1956.32	–	–

impregnation ratio and activation time > the interaction between activation temperature and activation time > activation temperature > the interaction between activation temperature and impregnation ratio.

3.1.2. Effect of operating variables on BET specific surface area

Fig. 2 demonstrates the interaction effects between the variables in contours and three-dimensional plots. Fig. 2(a) and (c) show the effect of impregnation ratio on specific surface area. The specific surface area was found to improve progressively with the increase of impregnation ratio and almost maintained stable with higher ratio. This phenomenon was attributed to the interaction between the activating agent and raw material, which could be explained as follows: (1) the diffusion of pyrophosphoric acid into the structure of *E. prolifra* can be promoted as a result of suitable increase of activating agent; (2) new channels (pores) can be produced due to more volatilisation of phosphorus compounds from activating agent pyrolysis; (3) the rupture of the carbon bridges may be caused by the surplus amount of activating agent; (4) an insulating layer around the raw material can be formed with the surplus activating agent and prevent the penetration of activating agent into the particles [10].

The effect of activation time on specific surface area is shown in Fig. 2(a) and (b). It can be seen that the specific surface area increased from 620 to 1,110 m²/g, with the activation time ranging from 30 to 60 min and then decreased with prolonged activation time. The sufficient activation time may lead to more pores formed inside the material. However, it was not necessary to prolong the activation time beyond a certain value. Cafer Saka et al. [22] have reported that the excessive activation time would cause external shrinkage and collapse of the carbon framework. According to the BBD model analysis, 48 min is a suitable time for activation in consideration of the specific surface area of the prepared carbons.

Fig. 2(b) and (c) illustrates the role of activation temperature in specific surface area. The specific surface area was found to increase rapidly with the temperature, with the maximum at 455°C, and then gradually decreased with further increase of the activation temperature. This phenomenon was because increasing temperature improved the release of low-molecular volatiles from the matrix structure, leading to development of pore. This pyrolysis volatilization process indirectly enhanced the numbers of pores and consequently improved the specific surface area. Whereas, the burn-offs of the existing pores could be generated as a result of higher activation temperature. Theydan et al. [23] reported that sintering effect at high temperature could cause the shrinkage of the char and realignment of the carbon structure, which resulted in reduced pore areas as well as volume.

3.1.3. Process optimization

According to the reported results, the optimum preparation parameters with high specific surface area were obtained using a numerical optimization method. The optimum conditions were identified as: impregnation ratio of 1.26, activation temperature of 455°C and activation time of 48 min. Table 3 shows that the experimental values were in good agreement with the predicted values from BBD model, with considerably small deviations between the actual and predicted values, which was only 2% for specific surface area.

(a)

(b)

(c)
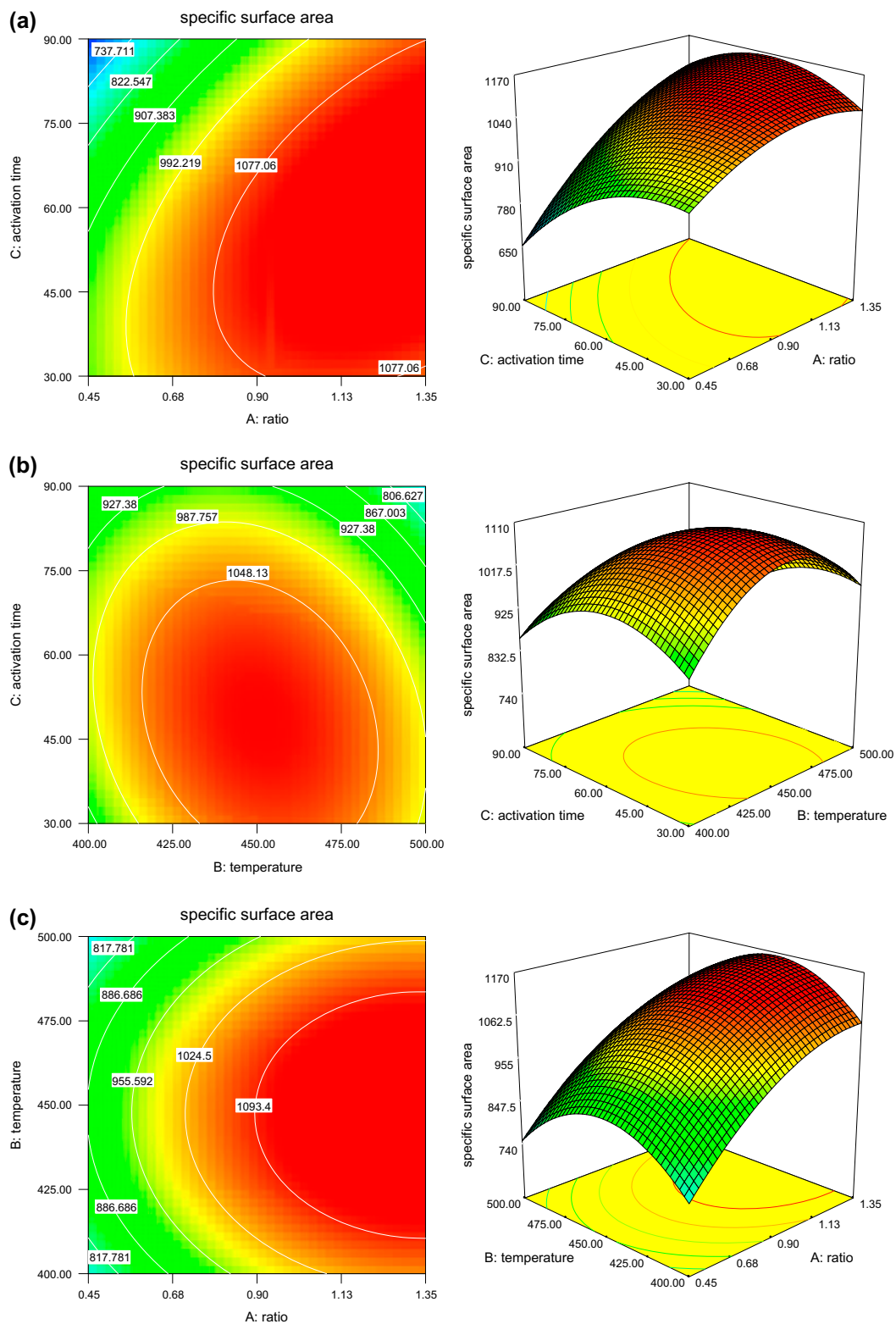
Fig. 2. Contours and three-dimensional response surface plots of specific surface area for EPAC: (a) effect of impregnation ratio and activation time, (b) effect of activation time and temperature, and (c) effect of impregnation and temperature.

3.2. Characterization of activated carbon prepared under optimum condition

3.2.1. Porous structure analysis

Fig. 3 shows the pore size distribution and adsorption–desorption isotherms of N_2 at 77 K for the carbon prepared under optimum condition. The isotherms possessed both type I and type IV isotherms in accordance with the porous structure parameters in Table 4, indicating the microporous–mesoporous structure of the prepared carbon. Moreover, the volume of micropores accounts for less than 20%, confirming their mainly mesoporous nature for the prepared carbons. The isotherm resembled an apparent hysteresis loop with the relative pressure increasing to 0.7, further implying the successful development of mesoporosity for the prepared carbons. This phenomenon demonstrated that pyrophosphoric acid, as an activating agent, had played an important role in the development of mesoporous for the raw materials. Table 5 provides a comparison of the adsorption capacities of carbons for methylene blue which were prepared by various precursors and activating agents [24–28]. The highest methylene blue (330 mg/g) demonstrated that the prepared carbons were developed in mesopores tremendously again.

3.2.2. Surface morphology analysis

Scanning electron microscopy (SEM) technique was introduced to observe the surface morphology of the raw precursor and activated carbon. Fig. 4(a) showed that *E. prolifra*, as green algae, possessed special hollow cellular wall structures. It can be obviously seen from Fig. 4(b) that there are some pores on carbon's surface. Those cavities were pronounced, uniform, honeycomb-like, resulting from the evaporation of impregnated pyrophosphoric acid derived compounds or chemical reaction between the raw precursor and activating agent, or the space formerly occupied by the activating agent.
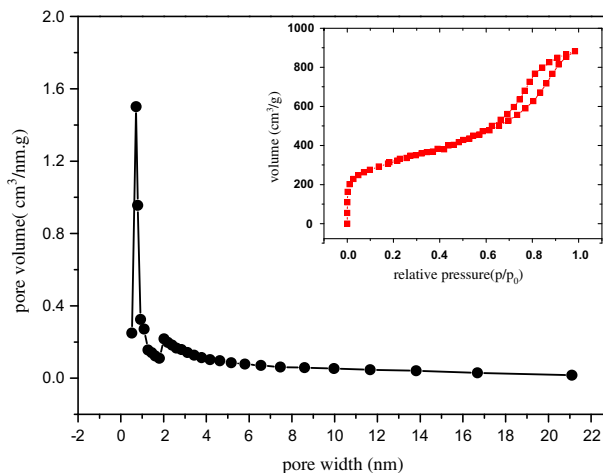
Fig. 3. Pore size distribution and adsorption–desorption isotherms of N_2 at 77 K for EPAC.

3.2.3. Fourier transformed infrared analysis

The properties of prepared carbons are not only related to the texture structure but also to the surface functional groups. The FT-IR spectra of activated carbon are presented in Fig. 5. It was shown that the broad bands around 3,400 cm^{-1} were attributed to the O–H stretching vibration of phenol, carboxylic and alcohol [29,30]. The bands around 1,564 cm^{-1} were derived from the C=O stretching vibration of carboxylic acid or quinone type structure, which was possible as a result of the extraction of OH groups or H element from the aromatic rings existing in the impregnation and heating treatment process owing to the dehydration of pyrophosphoric acid [20]. The sharp peaks at 1,417 cm^{-1} were associated with the vibration of –CH$_2$. The intense absorption peak at 1,110 cm^{-1} indicated the existence of P=O bond in phosphate esters or C–O bond in carboxylic [31–33]. Some weak bands also appeared around 500 cm^{-1}, which corresponded to the out-of-plane bending pattern of O–H or C–H group. The analysis above implied that there were some carbonyl and hydroxyl acidic functional groups on the surface of

Table 3
Process optimization validation

Parameter	Impregnation ratio	Activation temperature (℃)	Activation time (min)	BET specific surface area (m²/g)	
				Predicted	Experimental
Value	1.26	455	48	1,147	1,124

Table 4
Porous structure parameters of EPAC

Sample	S_{BET} (m^2/g)	S_{mic} (m^2/g)	(%)	S_{ext} (m^2/g)	(%)	V_{tot} (cm^3/g)	V_{mic} (cm^3/g)	(%)	V_{mec} (cm^3/g)	(%)	D_{AC} (nm)
EPAC	1,124.1	431.4	38.4	692.7	61.6	1.365	0.212	15.53	1.153	84.47	4.855

Table 5
Comparison adsorption capacities of methylene blue for various carbons

Precursor	Activation agent	Adsorption capacity (mg/g)	Reference
Enteromorpha prolifera	$H_4P_2O_7$	330	Present study
Piassava fibers	$ZnCl_2$	180	[28]
Rice straw	$(NH_4)_2HPO_4$	129	[27]
Durian peel	CO_2	284	[26]
Bamboo	H_3PO_4	286	[29]
Cotton stalk	KOH	294	[24]
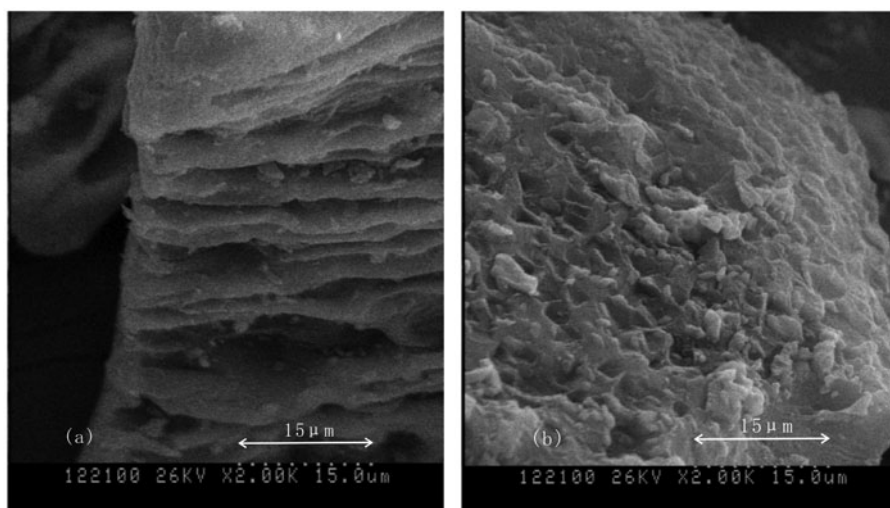
Fig. 4. SEM micrographs of (a) EP and (b) EPAC (2000×).

3.3. Adsorption experiments

3.3.1. Adsorption kinetics

The diagrams in Fig. 6 show the effect of CIP initial concentration and contact time on the adsorption of CIP onto EPAC. The CIP concentration decreased rapidly in the first 3 h, and then the equilibrium was gradually obtained within 6 h. It can also be realized that a longer time was required to reach equilibrium with the increase of CIP initial concentration due to the drastic competition of CIP molecules on the definite active sites of the adsorbents. As the initial concentration of adsorbate increased from 101 to 289 mg/L, the maximum removal rate was found to decrease from 100 to 74.5%. The removal rate was calculated according to the following equation:

$$Removal\ (\%) = \frac{q_e}{C_0 V} \times 100\% \tag{6}$$

where q_e (mg/g) and C_0 (mg/L) are the amount absorbed of CIP per unit mass of EPAC and the concentration of CIP at initial time. V is the solution volume (L). Because the adsorption capacity of the

prepared carbon, which may have some influence on adsorption.
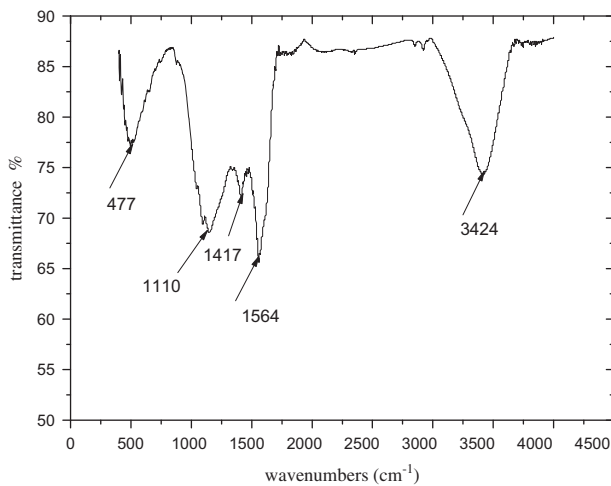
Fig. 5. FT-IR spectra of EPAC.
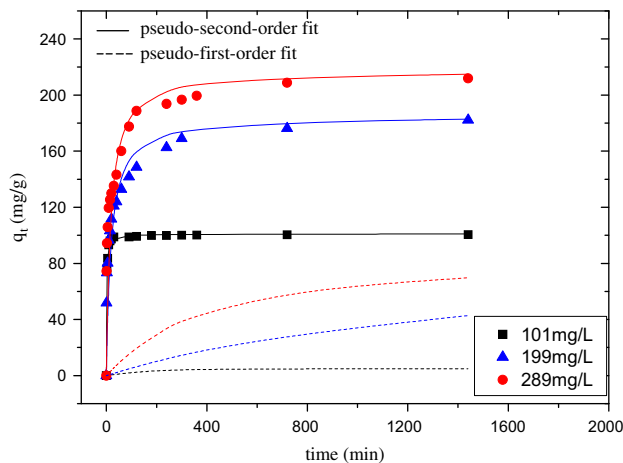
Fig. 6. Adsorption kinetics of CIP onto EPAC using nonlinear pseudo-first-order model and pseudo-second-order model.

adsorbing material was limited and constant, the activated carbon tended to saturate with the increase of the initial concentration of adsorbate. Hence, the maximum removal rate decreased from 100 to 74.5% while the initial concentration of adsorbate increased from 101 to 289 mg/L. In this study, the nonlinear curve-fittings of pseudo-first-order model, pseudo-second-order model and intra-particle diffusion model were introduced to understand the mechanisms of adsorption kinetic. The equations are expressed as follows:

$$q_t = q_e(1 - e^{-k_1 t}) \tag{7}$$

$$q_t = \frac{q_e^2 k_2 t}{1 + q_e k_2 t} \tag{8}$$

$$q_t = k_{pi} t^{1/2} + C \tag{9}$$

where k_1 (min^{-1}), k_2 (g/mg min) and k_{pi} are rate constants of pseudo-first-order, pseudo-second-order models and intra-particle diffusion model, and q_e and q_t represent the adsorption amount of CIP onto EPAC at the time of equilibrium and t. Table 6 clearly shows that the adsorption kinetic data were fitted by the pseudo-second-order model very well with a higher R^2 (>0.999). In addition, the values of calculated q_e agreed with the experimental data in the case of the pseudo-second-order kinetics, indicating the chemical adsorption progress involved valence forces through exchanging or sharing of electrons between adsorbate and sorbent [34,35]. Besides, the values of the second order rate constant k_2 decreased with the increasing initial CIP concentration, indicating that the lower sorption rates were obtained. This behaviour can be attributed to the more intense competition for the surface sorption sites at higher initial CIP concentrations. The intra-particle diffusion model was applied to investigate the adsorption process and understand the adsorption mechanism. The curve-fitting plots are demonstrated in Fig. 7 and the corresponding parameters are summarized in Table 6. It can be observed that the plots can be divided into two stages: a sharp rise stage and a mild rise stage. At the sharp rise stage, the diffusion of CIP was mainly restricted by the internal pore structure of the EPAC. At the mild rise stage, the diffusion of CIP was retarded by the formerly adsorbed molecules. The values of the intercept were not zero, revealing that the boundary layer

Table 6
Adsorption kinetic constants for the adsorption of CIP onto EPAC

C_0 (mg/L)	101.47	199.03	289.98
q_e(exp) (mg/g)	100.57	189.47	216.06
First-order kinetics			
$\quad k_1$ (min^{-1})	0.0061	0.0027	0.0010
$\quad q_e$(cal) (mg/g)	4.85	55.34	71.09
$\quad R^2$	0.7042	0.8790	0.6099
Second-order kinetics			
$\quad k_2$(g/mg min)	8.45×10^{-3}	2.95×10^{-4}	2.73×10^{-4}
$\quad q_e$(cal) (mg/g)	100.93	184.02	216.55
$\quad R^2$	1.0000	0.9998	0.9999
Intra-particle diffusion			
$\quad K_{p1}$ (mg/g min$^{1/2}$)	30.744	17.52	13.356
$\quad C$	8.5211	29.6	58.317
$\quad R^2$	0.9112	0.8652	0.8222
$\quad K_{p2}$ (mg/g min$^{1/2}$)	1.7286	3.6404	1.3013
$\quad C$	89.387	105.56	174.11
$\quad R^2$	0.9706	0.9901	0.9923

diffusion may be the rate-limiting step for CIP adsorption onto the EPAC. In addition, the intercept values increased with increasing initial CIP concentrations, implying that the effect of boundary layer diffusion on adsorption was more dominant at higher initial CIP concentration.

3.3.2. Adsorption isotherm

The analyses of adsorption isotherms data are the most important to elaborate the mechanism of the adsorption system. Therefore, Langmuir, Freundlich and Dubinin–Radushkevich isotherm models were applied to provide an insight into the adsorption behaviours. The Langmuir model assumes that the sorption process happens at specific homogeneous sites with no transmigration of adsorbate to the adsorbent surface [36]. The Freundlich model assumes that the sorption process occurs on heterogeneous surfaces with different binding energies for all adsorption sites [37]. The Dubinin–Radushkevich model assumes that the sorption process occurs on both heterogeneous and homogeneous surfaces [36]. The equations are described as follows:

$$\frac{C_e}{q_e} = \frac{1}{Q_m b} + \frac{1}{Q_m} C_e \tag{10}$$

$$R_L = \frac{1}{1 + bC_0} \tag{11}$$

$$\log q_e = \log K_F + (1/n) \log C_e \tag{12}$$

$$\ln q_e = \ln q_s - k_{ad}\varepsilon^2 \tag{13}$$
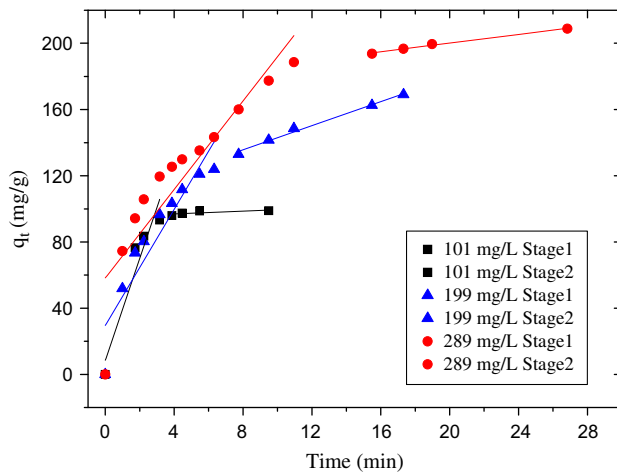
Fig. 7. Adsorption kinetics for CIP adsorption onto EPAC using intraparticle diffusion model.

$$\varepsilon = RT \ln(1 + 1/C_e) \tag{14}$$

$$E = 1/(2k_{ad})^{1/2} \tag{15}$$

where C_e (mg/L) is the concentration of CIP at equilibrium time. b (1/mg), K_F (mg/g(l/mg)$^{1/n}$), and k_{ad} (mol^2 kJ^{-2}) are the Langmuir, Freundlich and Dubinin–Radushkevich constants. Q_m and q_s (mg/g) are the monolayer adsorption capacity and theoretical saturation capacity of the adsorbent. R and T are the gas constant (8.314 J/mol K) and solution temperature (K).

The isotherm parameters and correlation coefficients were calculated and represented in Table 7. The highest monolayer adsorption capacity of 333 mg/g was comparable to what was reported on a commercial activated carbon sample, which demonstrated that EPAC was a considerably efficient adsorbent. The better adsorption capacity was attributed to the higher specific surface area and abundance of functional groups of the prepared carbons. It can be seen that the adsorption data of CIP could be best fitted by Langmuir isotherm model because its correlation coefficient was closest to one, compared with the Freundlich and Dubinin–Radushkevich models. This result reflected that homogeneous and monolayer adsorption was predominant and no steric hindrance and lateral interaction occurred between CIP and the absorbent. The value of dimensionless constant (R_L) reflects whether the type of isotherm is unfavourable ($R_L > 1$), or linear ($R_L = 1$) favourable ($0 < R_L < 1$), or irreversible ($R_L = 0$). Table 7 represents the calculated value of R_L was between 0 and 1, suggesting that the adsorption of CIP onto EPAC was favourable. The n value of Freundlich isothermal equation gives an indication on the favourability of the adsorption. The result shows that the value of n was 6.99, implying beneficial adsorption of CIP onto EPAC, which was in good agreement with the analysis above. E is the free energy change of adsorption, while one mole of adsorbate ions is transmitted from boundlessness in the solution to the surface of adsorbent. The value of E can give an indication of the adsorption mechanism. If the value of E lies in the range of 20–40 kJ/mol, this indicates chemisorption. If the value of E is between 8 and 16 kJ/mol, this indicates that adsorption occurred by ion-exchange. Whereas, if the value of E is between 1 and 8 kJ/mol, physical adsorption would be the most probable adsorption mechanism involved. In Table 7, the value of E (2.67 kJ/mol) was found between 1 and 8 kJ/mol, the adsorption mechanism involved in CIP onto EPAC was physical adsorption.

Table 7
Isotherm parameters for CIP adsorption onto EPAC at 293 K

Isotherms (constants)	Langmuir model				Freundlich model			Dubinin–Radushkevich model		
	Q_m (mg/g)	b (L/mg)	R_L	R^2	K_F (mg/g(l/mg)$^{1/n}$)	n	R^2	E (kJ/mol)	q_s (mg/g)	R^2
Values	333.3	0.4225	0.0046	0.9978	167.10	6.99	0.8420	2.6726	294.36	0.8869

3.3.3. Adsorption mechanisms

The solution pH may affect the surface charge properties of both adsorbent and adsorbate. Fig. 8(a) shows the influence of solution pH on the adsorption
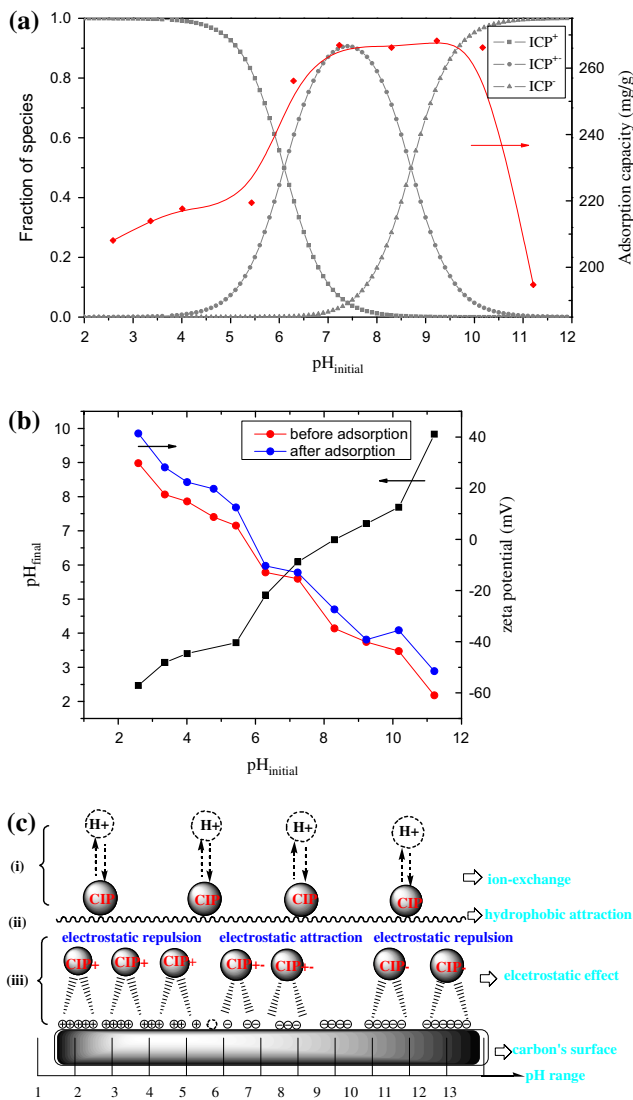
of CIP onto activated carbon. The amount of CIP uptake increased with increasing pH as pH was below 7 and remained almost constant in the pH range of 7–9. Nevertheless, the uptake amount decreased sharply from 268 to 194 mg/L in the pH range from 9–11. Fig. 8(b) and (c) demonstrate the zeta potential on the surface of carbon before and after adsorption and the involved crucial adsorption mechanisms, respectively. The adsorption mechanisms can be elucidated as follows: (1) the ion-exchange effect, which occurred in the whole adsorption process considering the existence of acidic functional groups as mentioned above; (2) the hydrophobic attraction, which was favourable to the adsorption; above-mentioned both functions could explain the adsorption behaviour, occurring during the whole pH range; (3) the electrostatic effect was the leading influential factor. Fig. 8(b) indicates that the number of positively charged adsorbent increased when the pH decreased gradually below 6 and meanwhile, the dominant forms of CIP at pH between 2 and 6 were CIP$^+$. Therefore, the electrostatic repulsion became drastic with the decrease of pH, leading to the decline of adsorption capacity. Similarly, the anionic form of CIP$^-$ was primarily present at pH above 9. Moreover, zeta potential showed that the increasing solution pH enhanced the negative charge strength of EPAC, resulting in the forceful electrostatic repulsion. Between pH 6 and 9, the prominent forms of CIP were CIP^{+-}, the surface charge of carbon was also mild, which is good for adsorption.

4. Conclusions

The results showed that *E. prolifra* was a promising raw material for the preparation of activated carbon and the pyrophosphoric acid was an excellent activating agent to produce mesoporous carbons. The response surface model was successfully applied to investigate the influences of pyrophosphoric acid impregnation ratio, activation time and activation temperature on the specific surface area of the activated carbons. The optimum preparation condition has been identified as temperature of 455°C, time of 48 min and impregnation ratio of 1.26, presenting carbons with a specific surface area up to 1,124 m²/g, total pore

Fig. 8. (a) Relative proportion of CIP solution speciation as a function of pH, (b) zeta potential of carbons in CIP solution, and (c) major mechanisms for sorption of CIP onto EPAC.

volume of $1.365\,cm^3/g$ and adsorption capacity of methylene blue of $330\,mg/g$. The resultant carbon was used for CIP adsorption. Adsorption kinetic could be successfully described by pseudo-second-order model and adsorption isotherm could be better described by Langmuir model. The ion-exchange, hydrophobic attraction and electrostatic effect were the main adsorption mechanisms.

Acknowledgments

References

[1] C. Wang, R.-C. Yu, M.-J. Zhou, Effects of the decomposing green macroalga Ulva *(Enteromorpha) prolifera* on the growth of four red-tide species, Harmful Algae 16 (2012) 12–19.

[2] A. Özer, G. Gürbüz, A. Çalimli, B.K. Körbahti, Biosorption of copper(II) ions on *Enteromorpha prolifera*: Application of response surface methodology (RSM), Chem. Eng. J. 146 (2009) 377–387.

[3] B. Li, S. Liu, R. Xing, K. Li, R. Li, Y. Qin, X. Wang, Z. Wei, P. Li, Degradation of sulfated polysaccharides from *Enteromorpha prolifera* and their antioxidant activities, Carbohydr. Polym. 92 (2013) 1991–1996.

[4] Z. Zhang, K. Wang, J.D. Atkinson, X. Yan, X. Li, M.J. Rood, Z. Yan, Sustainable and hierarchical porous *Enteromorpha prolifera* based carbon for CO_2 capture, J. Hazard. Mater. 229–230 (2012) 183–191.

[5] Q. Wu, Z. Li, H. Hong, K. Yin, L. Tie, Adsorption and intercalation of ciprofloxacin on montmorillonite, Appl. Clay Sci. 50 (2010) 204–211.

[6] Z. Li, H. Hong, L. Liao, C.J. Ackley, L.A. Schulz, R.A. MacDonald, A.L. Mihelich, S.M. Emard, A mechanistic study of ciprofloxacin removal by kaolinite, Colloids Surf. B. 88 (2011) 339–344.

[7] L. Huang, Y. Sun, W. Wang, Q. Yue, T. Yang, Comparative study on characterization of activated carbons prepared by microwave and conventional heating methods and application in removal of oxytetracycline (OTC), Chem. Eng. J. 171 (2011) 1446–1453.

[8] Q. Miao, Y. Tang, J. Xu, X. Liu, L. Xiao, Q. Chen, Activated carbon prepared from soybean straw for phenol adsorption, J. Taiwan Inst. Chem. Eng. 44 (2013) 458–465.

[9] Y. Li, Q. Du, T. Liu, Y. Qi, P. Zhang, Z. Wang, Y. Xia, Preparation of activated carbon from *Enteromorpha prolifera* and its use on cationic red X-GRL removal, Appl. Clay Sci. 257 (2011) 10621–10627.

[10] M.A. Nahil, P.T. Williams, Pore characteristics of activated carbons from the phosphoric acid chemical activation of cotton stalks, Biomass and Bioenergy 37 (2012) 142–149.

[11] F. Bouhamed, Z. Elouear, J. Bouzid, Adsorptive removal of copper(II) from aqueous solutions on activated carbon prepared from Tunisian date stones:

[12] A.L. Cazetta, A.M.M. Vargas, E.M. Nogami, M.H. Kunita, M.R. Guilherme, A.C. Martins, T.L. Silva, J.C.G. Moraes, V.C. Almeida, NaOH-activated carbon of high surface area produced from coconut shell: Kinetics and equilibrium studies from the methylene blue adsorption, Chem. Eng. J. 174 (2011) 117–125.

[13] Y. Gao, Q. Yue, B. Gao, Y. Sun, W. Wang, Q. Li, Y. Wang, Preparation of high surface area-activated carbon from lignin of papermaking black liquor by KOH activation for Ni(II) adsorption, Chem. Eng. J. 217 (2013) 345–353.

[14] Y. Gao, Q. Yue, B. Gao, Y. Sun, W. Wang, Q. Li, Y. Wang, Comparisons of porous, surface chemistry and adsorption properties of carbon derived from Enteromorpha prolifera activated by $H_4P_2O_7$ and KOH, Chem. Eng. J. 232 (2013) 582–590.

[15] R.-L. Tseng, S.-K. Tseng, F.-C. Wu, C.-C. Hu, C.-C. Wang, Effects of micropore development on the physicochemical properties of KOH-activated carbons, J. Chin. Inst. Chem. Eng. 39 (2008) 37–47.

[16] M.J. Ahmed, S.K. Theydan, Fluoroquinolones antibiotics adsorption onto microporous activated carbon from lignocellulosic biomass by microwave pyrolysis, Taiwan Inst. Chem. Eng. 45 (2014) 219–226.

[17] H. Liu, J. Zhang, N. Bao, C. Cheng, L. Ren, C. Zhang, Textural properties and surface chemistry of lotus stalk-derived activated carbons prepared using different phosphorus oxyacids: Adsorption of trimethoprim, J. Hazard. Mater. 235–236 (2012) 367–375.

[18] Y. Sun, Q. Yue, B. Gao, B. Wang, Q. Li, L. Huang, X. Xu, Comparison of activated carbons from *Arundo donax Linn* with $H_4P_2O_7$ activation by conventional and microwave heating methods, Chem. Eng. J. 192 (2012) 308–314.

[19] M.D.G. de Luna, E.D. Flores, D.A.D. Genuino, C.M. Futalan, M.-W. Wan, Adsorption of Eriochrome Black T (EBT) dye using activated carbon prepared from waste rice hulls – Optimization, isotherm and kinetic studies, J. Taiwan Inst. Chem. Eng. 44 (2013) 646–653.

[20] Z.-Y. Zhong, Q. Yang, X.-M. Li, K. Luo, Y. Liu, G.-M. Zeng, Preparation of peanut hull-based activated carbon by microwave-induced phosphoric acid activation and its application in Remazol Brilliant Blue R adsorption, Ind. Crops Prod. 37 (2012) 178–185.

[21] S.A.C. Carabineiro, T. Thavorn-amornsri, M.F.R. Pereira, P. Serp, J.L. Figueiredo, Comparison between activated carbon, carbon xerogel and carbon nanotubes for the adsorption of the antibiotic ciprofloxacin, Catal. Today 186 (2012) 29–34.

[22] C. Saka, BET, TG–DTG, FT-IR, SEM, iodine number analysis and preparation of activated carbon from acorn shell by chemical activation with $ZnCl_2$, J. Anal. Appl. Pyrolysis 95 (2012) 21–24.

[23] S.K. Theydan, M.J. Ahmed, Optimization of preparation conditions for activated carbons from date stones using response surface methodology, Powder Technol. 224 (2012) 101–108.

[24] H. Deng, G. Li, H. Yang, J. Tang, J. Tang, Preparation of activated carbons from cotton stalk by microwave assisted KOH and K_2CO_3 activation, Chem. Eng. J. 163 (2010) 373–381.

[25] Q.-S. Liu, T. Zheng, N. Li, P. Wang, G. Abulikemu, Modification of bamboo-based activated carbon using microwave radiation and its effects on the adsorption of methylene blue, Appl. Surf. Sci. 256 (2010) 3309–3315.

[26] K. Nuithitikul, S. Srikhun, S. Hirunpraditkoon, Influences of pyrolysis condition and acid treatment on properties of durian peel-based activated carbon, Bioresour. Technol. 101 (2010) 426–429.

[27] P. Gao, Z.-H. Liu, G. Xue, B. Han, M.-H. Zhou, Preparation and characterization of activated carbon produced from rice straw by $(NH_4)_2HPO_4$ activation, Bioresour. Technol. 102 (2011) 3645–3648.

[28] F.F. Avelar, M.L. Bianchi, M. Gonçalves, E.G. da Mota, The use of piassava fibers (Attalea funifera) in the preparation of activated carbon, Bioresour. Technol. 101 (2010) 4639–4645.

[29] Q.-S. Liu, T. Zheng, P. Wang, L. Guo, Preparation and characterization of activated carbon from bamboo by microwave-induced phosphoric acid activation, Ind. Crops Prod. 31 (2010) 233–238.

[30] H. Zhang, Y. Tang, D. Cai, X. Liu, X. Wang, Q. Huang, Z. Yu, Hexavalent chromium removal from aqueous solution by algal bloom residue derived activated carbon: Equilibrium and kinetic studies, J. Hazard. Mater. 181 (2010) 801–808.

[31] N. Rambabu, R. Azargohar, A.K. Dalai, J. Adjaye, Evaluation and comparison of enrichment efficiency of physical/chemical activations and functionalized activated carbons derived from fluid petroleum coke for environmental applications, Fuel Process. Technol. 106 (2013) 501–510.

[32] A.M.A. Nada, A.A. El-Gendy, S.H. Mohamed, Banana leaves as adsorbents for removal of metal ions from waste water, Carbohydr. Polym. 82 (2010) 1025–1030.

[33] T. Santhi, A.L. Prasad, S. Manonmani, A comparative study of microwave and chemically treated Acacia nilotica leaf as an eco friendly adsorbent for the removal of rhodamine B dye from aqueous solution, Arab. J. of Chem. (in press).

[34] F. Ahmad, W.M.A.W. Daud, M.A. Ahmad, R. Radzi, Cocoa (Theobroma cacao) shell-based activated carbon by CO_2 activation in removing of Cationic dye from aqueous solution: Kinetics and equilibrium studies, Chem. Eng. Res. Desn. 90 (2012) 1480–1490.

[35] K.Y. Foo, B.H. Hameed, Preparation, characterization and evaluation of adsorptive properties of orange peel based activated carbon via microwave induced K_2CO_3 activation, Bioresour. Technol. 104 (2012) 679–686.

[36] K.Y. Foo, B.H. Hameed, Insights into the modeling of adsorption isotherm systems, Chem. Eng. J. 156 (2010) 2–10.

[37] H. Chen, J. Zhao, G. Dai, J. Wu, H. Yan, Adsorption characteristics of Pb(II) from aqueous solution onto a natural biosorbent, fallen Cinnamomum camphora leaves, Desalination 262 (2010) 174–182.